ERRATA

UCB/ERL M84/64

Page 28 has the figures misnumbered. They should be changed from 14, 10, 15, 16, 16 to 2, 12, 1, 1, 1.

C. K. Birdsall

SIMULATION OF QUIET START MAGNETIZED PLASMAS, INCLUDING MAXWELLIAN AND VELOCITY-SPACE RING DISTRIBUTIONS

by

Kirk P. Kenyon

Memorandum No. UCB/ERL M84/64

27 July 1984

ELECTRONICS RESEARCH LABORATORY

College of Engineering
University of California, Berkeley, CA 94720

Simulation of Quiet Start Magnetized Plasmas, Including Maxwellian and Velocity-Space Ring Distributions†

Kirk P. Kenyon

ABSTRACT

Longitudinal electrostatic waves are simulated in a magnetized plasma, propagating perpendicular to B_o. Groups of particles are arranged in one or more rings and spokes in velocity space. Using various loading schemes to represent different particle velocity-space distributions in the simulations, $f(v_\perp)$, these particles are then distributed uniformly in position space along the length of the system. In particular, the evolution of magnetized cold and warm rings are followed (physically unstable), and of a magnetized Maxwellian (unstable due to the paticle loading) through to saturation. Rules are deduced for useful loading methods.

ACKNOWLEDGMENTS

I would like to acknowledge Professor Charles K. Birdsall and Dr. Thomas L. Crystal in the Electronics Research Laboratory at the University of California at Berkeley for their invaluable advice and suggestions during the course of this project. Credit should also be given to Dr. A. Bruce Langdon at the Lawrence Livermore National Laboratory as the author of the **ES1** code which was used in this project. I would also like to thank Stéphane Rousset for his help in writing this report on the Unix system.

The computational portion of this work was supported by the National Magnetic Fusion Energy Computer Center at the Lawrence Livermore National Laboratory. This report has been written using the UNIX† time-sharing system operated by the Computing Services at the University of California at Berkeley.

---

† Submitted in partial satisfaction of the requirements for the degree of Master of Science (Plan II) in Electrical Engineering in the Graduate Division at the University of California at Berkeley, April 1983.

† UNIX is a trademark of Bell Laboratories.

CONTENTS

1. INTRODUCTION

The objective of this report will be to present observations of the behavior of different loading schemes which were tried, and to comment on simulation results with respect to applicable theory. The main concern will be to find the loading scheme or schemes which most closely reproduce the predictions of analytic theory. The problems considered will progress from a one-ring Dory Guest Harris (DGH) instability, to a number of equally weighted, unequally spaced rings meant to approximate a physically stable Maxwellian distribution, then to a fully random loading of a Maxwellian distribution. The *number* of rings and spokes used and the particle *loading method* will be varied; resulting characteristics examined will include the initial quietness, the instability growth rates and the saturation level of the field energy. Finally, these characteristics will be compared with those derived from theory.

An ideal "quiet loading" scheme should start off with total electrostatic field energy at a very low level, ie. with modes excited only by round-off errors. When this initial excitation is followed by very low growth rate unstable modes, then such a "quiet loading" start should allow some time before the field energy rises to a thermal level, that is, saturates. A practical simulation run requires some "reasonable number" of particles to be quiet; it turns out that in 1½ or more dimensions, the number can be quite large.

2. THE MODELS

2.1. The Physical Model

The model used in the simulation consists of a magnetized plasma, assumed to be spatially uniform (homogeneous) both in the direction of the magnetic field and perpendicular to it; in the third, mutually perpendicular direction periodicity of length L is imposed. The model simulates only wave modes propagating perpendicular to the magnetic field.

The particles are of only one species, electrons in this case, though the sign of the charges is not important. There is no gravitational field. The particles move only in response to their own collective electrostatic fields and to the external magnetic field. Collisions between particles occur, and are not enhanced by added scattering. There is a neutralizing background of immobile charges.

A comparison of the two distributions to be modeled appears in Figure 1. A plot of both $f(v_\perp)dv_\perp$ and $f(v_x)dv_x$ are shown for the single ring distribution and the Maxwellian distribution.

2.2. The Numerical Model

The code used for this project is a version of **ES1**, which was originally written by A. B. Langdon, with changes made only in the loading and diagnostic options. These changes will be described in the next section. In brief, the **ES1** code keeps track of the particle positions and velocities at discrete instants of time, using this information to calculate their future velocities and positions. Particle velocities and positions are advanced in time knowing only the present velocities and positions; these determine the self-consistent electric field as generated from the present net charge distribution.

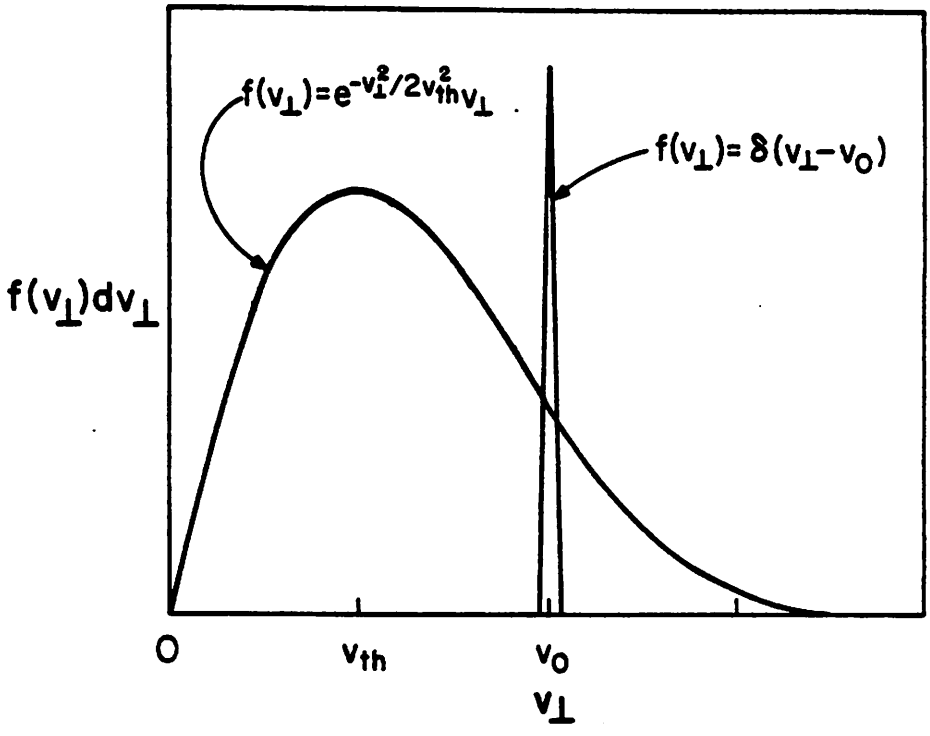

(a)

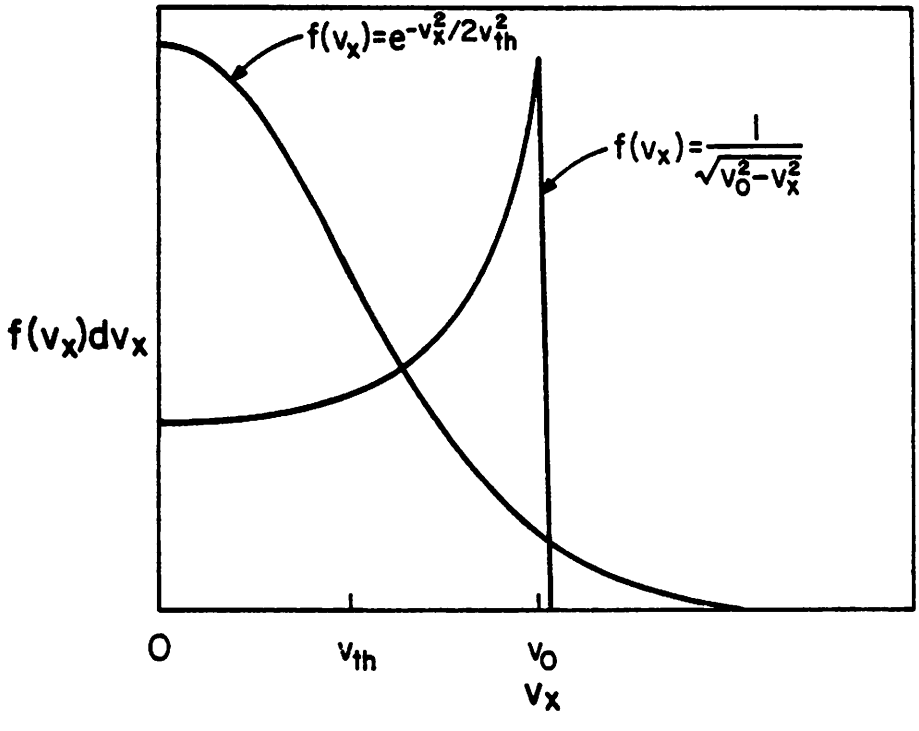

(b)

Fig. 1. (a) Distribution functions for Maxwellian and ring; (b) projections of the distributions on the v_x axis.

3. THE ES1 CODE

3.1. The Original Code

The original **ES1** code basically is made up of the main program and six subroutines; HISTRY, INIT, FIELDS, SETV, ACCEL and MOVE. The first subroutine, HISTRY, is called every timestep; its function is to *record* the various computed quantities, such as thermal energy, kinetic energy, field energy, etc., and to *plot* these records every five hundred timesteps. The first call of HISTRY is just to zero all of the arrays at the beginning of the run.

After the first HISTRY call, the subroutine INIT is called. INIT contains the loader, which establishes the initial positions and velocities of the particles, as determined by the choice of loading options. INIT also establishes a uniform, fixed, neutralizing charge (necessary when only one species is being used, as in all cases considered in this project). This is equivalent to loading a second species having an infinite mass while the species of interest is mobile.

FIELDS is then called to compute the initial electric field and potential. FIELDS also records the energies of specified modes and does any necessary snapshot plotting (see Sec. 3.3 below).

Because the positions of the particles are known at the times $t = n \cdot \Delta t$, while the velocities of the particles are known at $t+\Delta t/2$, the velocities of the particles must initially be moved backwards a half timestep. This function is carried out by the subroutines SETV and ACCEL.

The timestep loop now begins, in which the snapshots are plotted and the particle velocities advanced with the subroutine ACCEL. The particle positions are then advanced with the subroutine MOVE after which FIELDS calculates the new electric field and potential from the new particle positions. After the timestep loop has been cycled through *nt* times, it is exited and HISTRY is called to plot the last history plots.

3.2. The Loading Options

When the particles are loaded in INIT, there are three coordinates over which they must be distributed: x, v_x and v_y. Or, since there is axial symmetry about the magnetic field, the three coordinates can also be considered as x, v_p and θ_v, representing position, perpendicular velocity and gyrophase angle respectively. The distribution of the groups in v_p is determined by the type of velocity distribution chosen. The several types of velocity distributions considered in this paper all consist of one or more rings, equally weighted when there is more than one. The term "ring" is used in this report to mean a collection one or more particles, all of which have the same perpendicular velocity (v_p or $v_\perp$).

The parameters *lx* and *lthv* control the manner in which the particles are loaded in the position and the gyrophase angle dimensions, respectively. The loading options available are: bit-reversed, trit-reversed, random and ordered, corresponding to values for *lx* and *lthv* of 0,1,2 and 3, respectively. *Bit−reversed* is a binary based loading scheme for scrambling the position or velocity of the particles with respect to the number of the particles, as explained in more depth in QPR IV 1980[1] and below. *Trit−reversed* is identical to bit-reversed, except that it is trinary based, (using base three instead of base two). The *random* loading scheme uses a random number generator whose seed may be set beforehand. By using different seeds we can reduce possible correlations between different coordinates. If this precaution were not taken, the *random-random* option simulation results would be the same as if the *ordered* option were used in one of the two coordinates. The *ordered* option gives each particle a position (or velocity) which is proportional to its subscript number.

The parameter *nlg* controls the number of 'loading groups'. When *nlg* is greater than one, the first n/nlg particles are loaded into the system from $x = 0$ to $x = l/nlg$. This loading

is then replicated in space to fill the rest of the system.

Successive particles along the length of the system can by rotated or "twisted" in their gyrophase angle with the parameter *tw*. Depending on the value chosen for *tw*, there will be either "no twist", a "distributed twist" or the loading groups will be "twisted individually". When a distributed twist is chosen, the amount of change in the gyrophase angle will be proportional to the position and the total twist along the length of the system equal to $-tw$. When the loading groups are twisted individually, each loading group is twisted as a whole, the amount being proportional to the position of the particle in the group farthest from $x = 0$, and with the total twist equal to *tw*. No twist is chosen when $tw = 0$. Figure 2 shows a typical loading arrangement consisting of 2 rings and 8 spokes. The relation between the position, perpendicular velocity and gyrophase angle are all indicated in the Figure. The distributed twist option is shown, for a $tw = -0.25$.

Since it was not practical to write one version of INIT which could produce all of the possible loading combinations, a second version of INIT was written which could produce a loading scheme that was thought to be promising. This scheme has been called the 'rings and spokes' loading, though it is possible to produce a very similar loading with the original version of INIT. In the 'rings and spokes' loading scheme there are one or more particles at each intersection in v_p, θ_v space, though they will have different positions in x space. In this version of INIT, the number of spokes is set by the parameter *nplg*, the number of rings is set by the parameter *nvlg*, and the total number of particles, n, divided by *nvlg* and *nplg* is the number of particles at each spoke-ring intersection, or "beam". In this report, a "beam" will refer to a set of one or more particles which have the same (v_p, θ_v) coordinates.

The arrangement of the particles along the length of the system can be selected through *lx*. As previously, the options available are: bit-reversed, trit-reversed, random and ordered.

3.3. The Diagnostics

The diagnostics in the original **ES1** code fall into two general categories: *snapshots* are plots at regular intervals of time during the simulation run; *histories* are running plots versus time. The original snapshot diagnostic options included: ϕ vs. x, E vs. x, ρ vs. x, v_x vs. x, v_y vs. v_x and $f(v_x)$. As the name implies, these diagnostics are records of the state of the particles at a specific time. Exactly when the snapshots are to be taken is determined by the value given the appropriate control parameters. If a value of m is given, for example, then a snapshot is taken every m timesteps beginning at $t = 0$.

The second type of diagnostic in the original **ES1** code, the history plots, are time plots (histories) of particular quantities which are of interest. These history plots are plotted every 500 timesteps, or at the end of the run, whichever comes first. The history plots of interest are: the field energy, the kinetic energy, the drift energy, the thermal energy, the total energy, and the mode energies. The field energy is the sum of all the spatial fourier mode energies; the energies of selected spatial modes can also be individually plotted as an option.

3.3.1. New Diagnostics

Three new snapshot options were added. Two of these were (1) the perpendicular velocity distribution function $f(v_p)$ and (2) the phase space v_p vs. x. The third new snapshot was of the energies of the various spatial modes plotted vs. the mode numbers. All the spatial modes from the first through highest selected are plotted, the highest being set by the value of the parameter *modmax*. Since there is a certain amount of variation in the mode energies from timestep to timestep, an average is taken over several timesteps previous to the one on which the plot is made. The number of timesteps over which the average is taken is determined by the value of the parameter *mav*. Spatial mode energy plots should not be requested closer together than the time over which the average is taken.

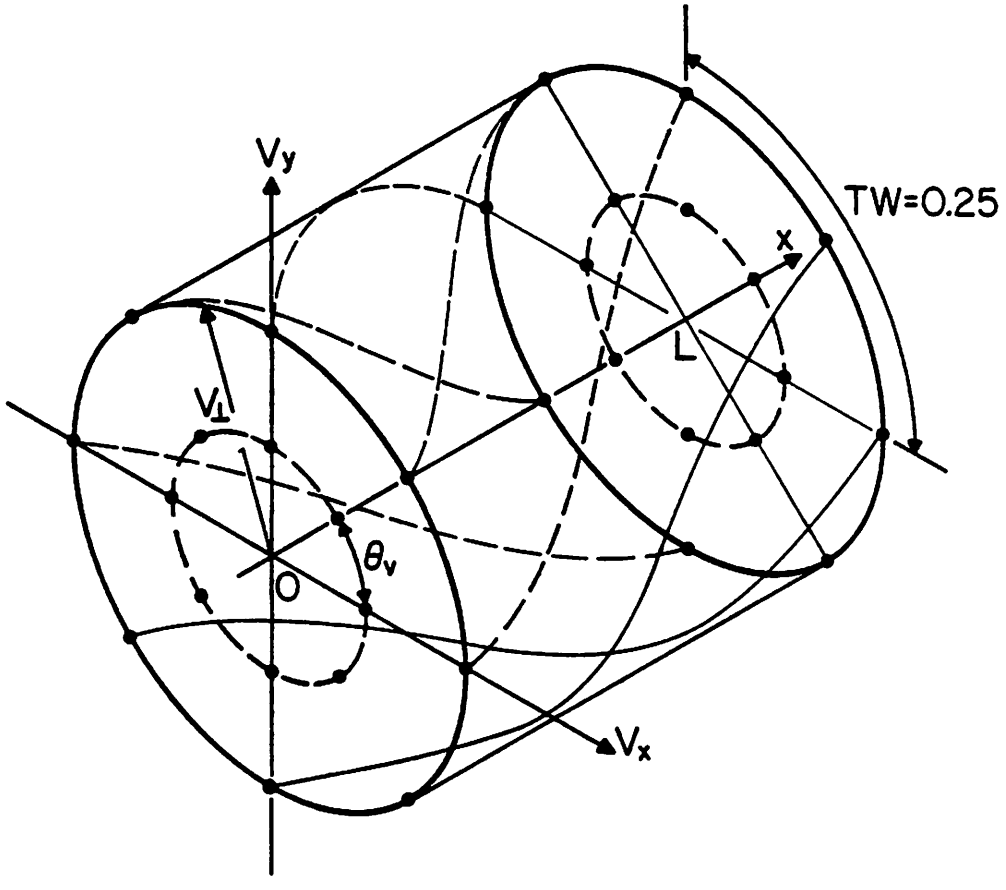

Fig. 2. Loading of 2 rings with 8 spokes, with a twist.

4. THE DORY-GUEST-HARRIS RING INSTABILITY RESULTS

The instability discussed by *Dory, Guest and Harris* [2] can occur when an infinite, homogeneous magneto-plasma has a "ring" shaped velocity distribution function $f(v_\perp, v_\parallel)$ which vanishes at $v_\perp = 0$. The unstable modes considered in their article were those with $k_\parallel = 0$, and could include a mode with the frequency equal to zero (purely growing). The simplest distribution function which satisfies this criterion is a single velocity ring: $f(v_\perp, v_\parallel) = (1/2\pi v_\perp)\delta(v_\perp - \alpha)\delta(v_\parallel)$. With this distribution function, the various possible growing modes will be unstable only if the quantity $b = k_\perp v_\perp/\omega_c$ has certain values. For the purely growing mode to occur, b must lie in any of the following ranges: $2.40 \leqslant b \leqslant 3.83$, $5.52 \leqslant b \leqslant 7.02$ ... $c_n \leqslant b \leqslant d_n$ where c_n is the nth zero of $J_0(b)$ and d_n is the nth zero of $J_1(b)$. If in addition to the above, the condition

$$\left(\frac{\omega_c}{\omega_p}\right)^2 < \frac{1}{b}\frac{d}{db}J_0^2(b)$$

is satisfied, then the plasma is unstable. For other modes, (those with non-zero frequencies), to be unstable, b must lie in different ranges as explained in the next section.

The authors then show that if the cold ring is given a thermal width v_{th}, then stability is improved; the instability threshold value of ω_p/ω_c increases with $v_{th}/\langle v_\perp \rangle$. A graph of the predicted variation of threshold ω_p/ω_c vs. the half-width of the distribution function, $v_{th}/\langle v_\perp \rangle$, for the zero-frequency mode is reproduced from *Dory, Guest and Harris* as Figure 3. The results of efforts to simulate both of these aspects of the Dory-Guest-Harris (DGH) instability will be presented in the next three sections.

4.1. The Cold Ring

A suitable approximation to a cold ring, ($v_{th} = 0$), was loaded and the simulation results were compared with DGH theory. Values chosen for the input parameters were as follows: n(number of particles) = 4096, $\omega_c = 0.2$, $L = 3.14$, $ng = 64$, $qm = 1.0$ and $v_o = 0.3$. The value of ω_p was then varied from 0.5 to 1.2, with the result that the ring became unstable with ω_p at about 0.57, or $\omega_p/\omega_c \approx 2.8$, which corresponds to a higher mode ($\omega \neq 0$). The mode in fact had $\omega/\omega_c = 2.5$ and $k = 4$ so $b = 6$. This satisfies the criteria presented in *Dory, Guest and Harris* that for a wave with frequency $n < \omega/\omega_c < n+1$ to be unstable, it is necessary that $j_{n,m} < b < j_{n+1,m}$, where $j_{n,m}$ is the mth zero of J_n. In this case the zeros of J_n which are of interest are the first zeros of J_2 and J_3, (5.136 and 6.380 respectively), which bracket $b = 6$.

Therefore the growing mode observed was indeed a legitimate mode whose parameters conformed to those predicted by *Dory, Guest and Harris.* The growth rates γ/ω_c vs. ω_p/ω_c are presented in Figure 4a for both the cold ring and various warm rings, as discussed in the next section. This growing mode is also in conformance with the results derived in the article by *Tataronis and Crawford*[3], where it was shown that as ω_p^2/ω_c^2 increased, the first unstable mode was in the frequency band $2 < \omega/\omega_c < 3$. The critical instability threshold value of ω_p^2/ω_c^2 was calculated to be 6.62, which corresponds to $\omega_p/\omega_c = 2.57$. The difference between the observed critical ω_p^2/ω_c^2 and that derived in *Tataronis and Crawford* may be attributed to the discreteness of the allowed k values.

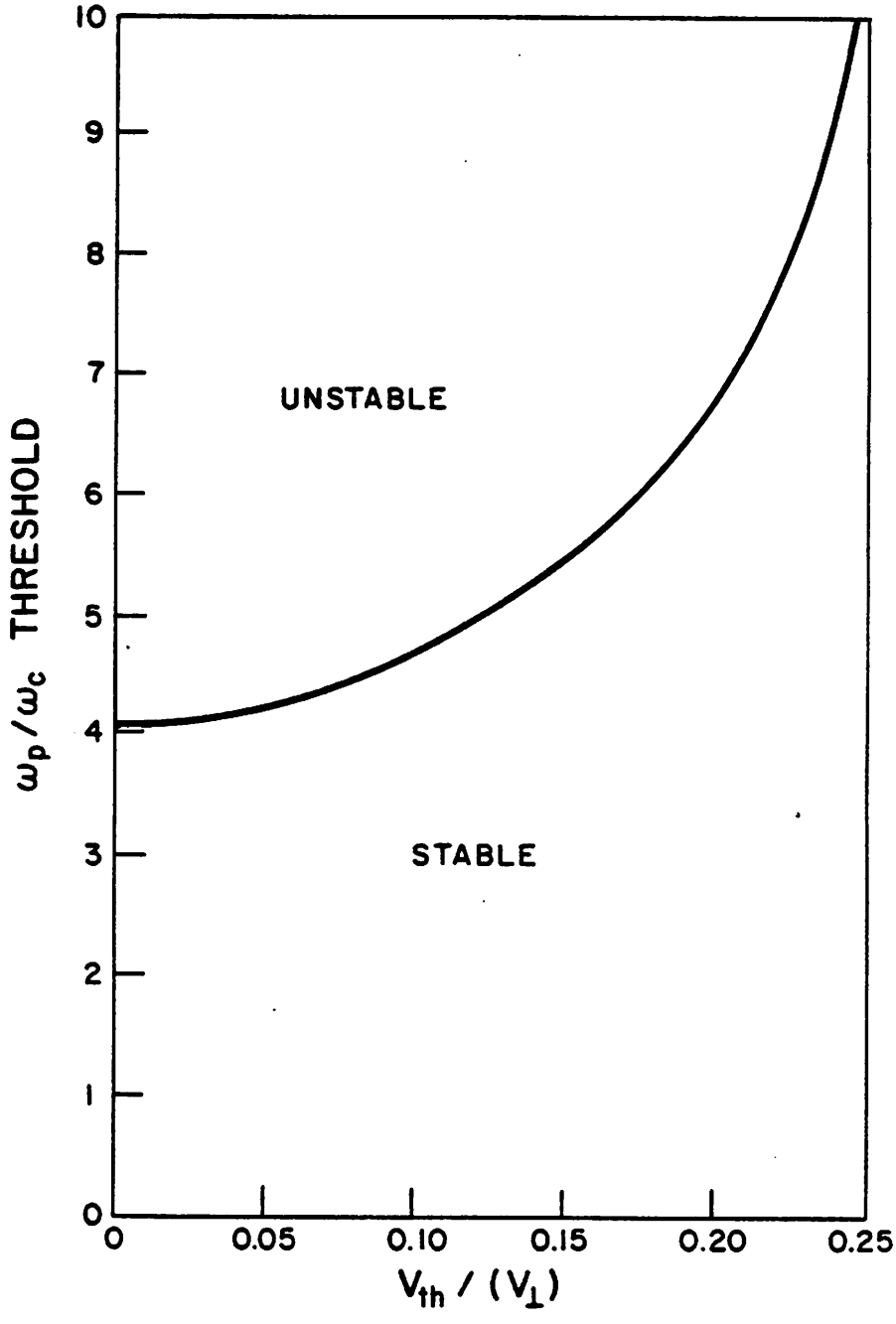

Fig. 3. Density threshold vs. half-width of the distribution for the zero-frequency DGH mode.

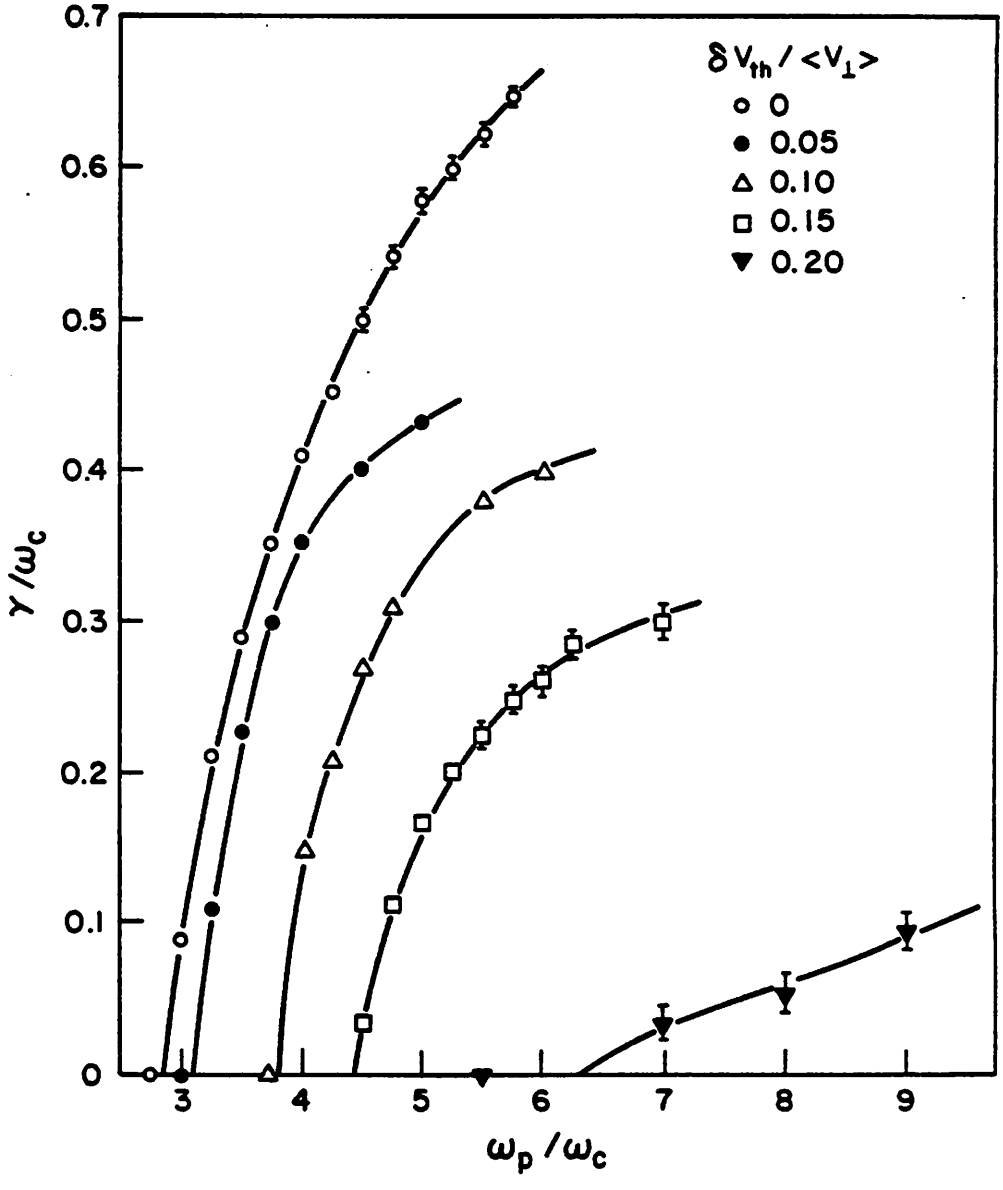

Fig. 4a. Growth rate vs. density for various cold and warm rings.

4.2. The Warm Ring

A warm ring was then loaded and the value of ω_p was varied to find the new threshold value of ω_p/ω_c for which the ring was unstable. The warmth of the ring was adjusted using $vt2$ so that several different threshold values could be found for rings of different degrees of warmth. Values of $vt2$ were chosen so that $v_{th}/<v_\perp>$ was equal to 0.05, 0.10, 0.15, and 0.20. The threshold value for stability increased with the increased thermal spread of the ring, as predicted in *Dory, Guest and Harris.* The increase in stability is slight at first,but then increases more rapidly after $v_{th}/<v_\perp>$ becomes more than approximately 0.10, as is shown in Figure 4b.

Because of the thermal spread of the warm ring, more simulation particles were needed to represent the distribution adequately. For this reason the number of particles was increased in the warm ring simulation to $n = 8192$ ($n = 16384$ was also tried but as the improvement was not significant enough to justify the increased expense, $n = 8192$ was used). As v_{th} was increased, with n/nlg held constant, the quality of the simulation of the warm ring decreased, ie. the plots were noisier and the growth rates were not as well defined. A few runs were made with larger n/nlg, but the variation of the simulation results with n/nlg was not sufficient to merit increasing n further.

In **ES1**, due to the finite spatial grid, only discrete spatial (Fourier) modes exist. The maximum spatial mode number (minimum wavelength) m which the code can simulate is limited by the grid spacing; the smallest wavelength the grid can detect is $\lambda_{min} = 2L/ng$. In general the wavelength of the mth mode is $\lambda_m = L/m$, so this maximum spatial mode is: $m_{max} = ng/2$. The minimum mode number ($m = 1$) corresponds to the maximum wavelength: $\lambda_1 = L$. Since $k = 2\pi/\lambda$, then in general $k_m = 2\pi m/L$.

Care was taken to ensure that the k value of the growing mode fell on or near an allowed mode number. This was necessary because if the most unstable mode had a k value which corresponded to an m value which was not allowed (either because it was not an integer or it was too large), then it would not grow. Initially mode 2 was the growing mode which corresponded to $k = 4$, but as the thermal spread was increased to $v_{th}/<v_\perp> = 0.15$, mode 1 became the growing mode. This indicated that the value of k was changing. To determine k more accurately it was necessary to increase the resolution of k by decreasing $2\pi/L$ since as shown above, k was an integral multiple of $2\pi/L$. The only way to increase the resolution of k was to increase L.

To determine more accurately what value k was, L was increased to 16π, whereupon the primary growing mode was $m = 24$, which corresponded to $k = 3$. In addition to increasing the resolution of k, the total number of allowed modes must also be increased, otherwise the desired k value may no longer be covered by the range of allowed m values. This was accomplished by increasing the number of grid cells, loading groups and particles (ng, nlg and n, respectively) by the same factor that L was increased by.

A measure of how closely spaced the kv_{th}/ω_c values are can be obtained by calculating the value of $k_1 v_{th}/\omega_c$. With the typical values of $L = 4\pi$, $v_o = 0.3$, and $\omega_c = 0.2$, then $k_1 v_{th}/\omega_c = 0.75$. The value for v_o is used here for v_{th} since this is a ring distribution in which the thermal spread is small compared to the ring velocity.

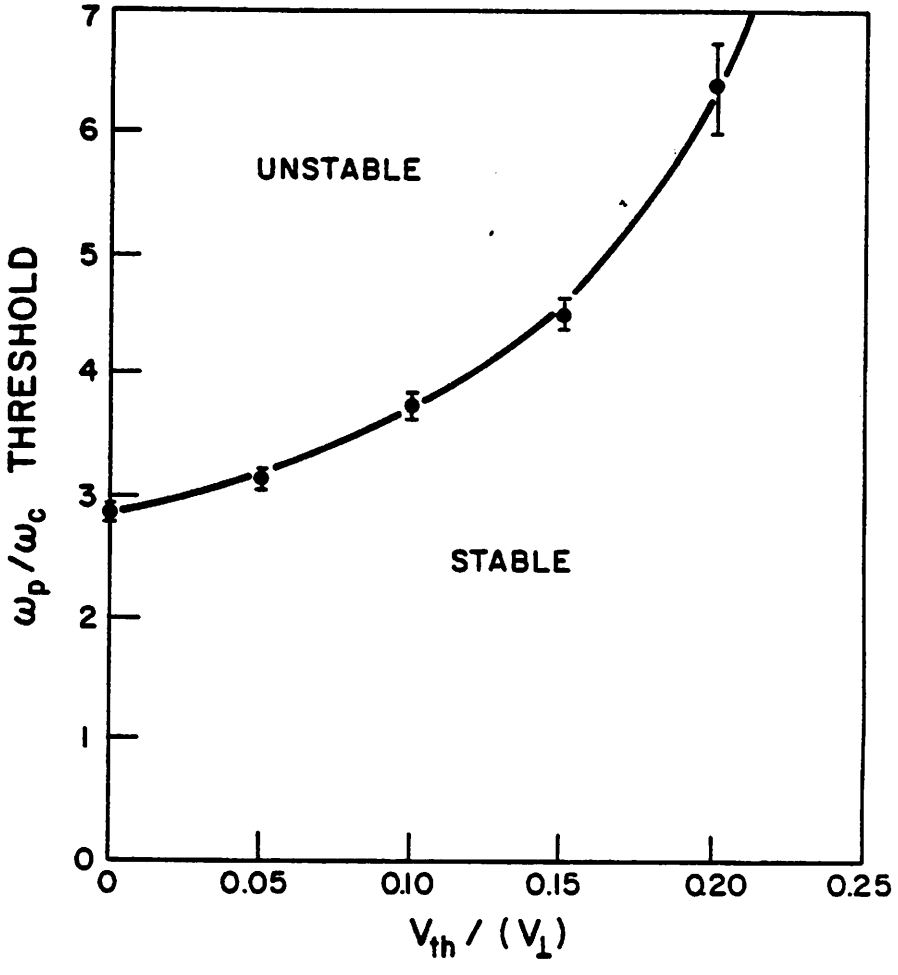

Fig. 4b. Simulation results for cold and warm ring threshold.

4.3. The Loading Schemes

For the ring configuration, (cold and warm), the original version of INIT was used almost unaltered. The number of loading groups was set equal to the number of cells ($nlg = ng$) so that at each (v_x, v_y) location there would be one particle per cell in each "beam" on the average. This prevented the grid from seeing the regularity which is present since the grid cannot resolve a mode number equal to or higher than the number of cells. Fewer particles per cell would result in a large amount of energy in a mode corresponding to $ng \times$(particles/cell). This excited mode would usually not be a growing mode and thus would remain at its initial level but its presence would obscure the other, growing modes in the total field energy plot. Particles per cell here refers only to those particles which all have the same initial (v_x, v_y).

The particles were then loaded into position space with the *bit−reversed* option, while they were loaded in gyrophase with the *ordered* option. The duplication of the first loading group into the rest of the system introduces a certain amount of regularity, but no two collections of particles, each at different (v_x, v_y), occupy the same positions in x-space. In this loading scheme the thermally spread ring is made up of n/nlg rings, each ring consisting of only one 'spoke' with the gyrophase angle of the spokes arranged in a bit-reversed manner. Thus, no two rings have their spokes at the same gyrophase angle.

5. THE QUIET START MAXWELLIAN RESULTS

In simulating a quiet start Maxwellian distribution, two different loading schemes were used. The first was the 'rings and spokes' scheme in which there were a number of rings, each of which consisted of some number of particles. When the particles were arranged so that there was one particle from each ring at each gyrophase angle, the effect of "spokes" in (v_p, θ_v) space was given. Thus, particles which were in different rings (different v_p), but had the same gyrophase angle (θ_v) were in the same spoke.

5.1. The Unmagnetized Maxwellian

The case where the magnetic field is zero was treated by *Gitomer and Adams*[4]. They studied two different schemes for loading a Maxwellian velocity distribution: (1) equally weighted but unequally spaced beams and (2) equally spaced but unequally weighted beams. In this unmagnetized case the 'rings' become beams, (there is no v_y). The first loading scheme was relevant to my work as a limiting case as the magnetic field goes to zero. This equally weighted beam case was simulated using approximately the same parameters as in *Gitomer and Adams.* It was found that those beams with the highest velocity were the most unstable, thus reproducing results obtained by *Gitomer and Adams.* The growth of the electric field energy and a v vs. x phase space plot after growth has proceeded sufficiently to be visible are presented here in Figure 5.

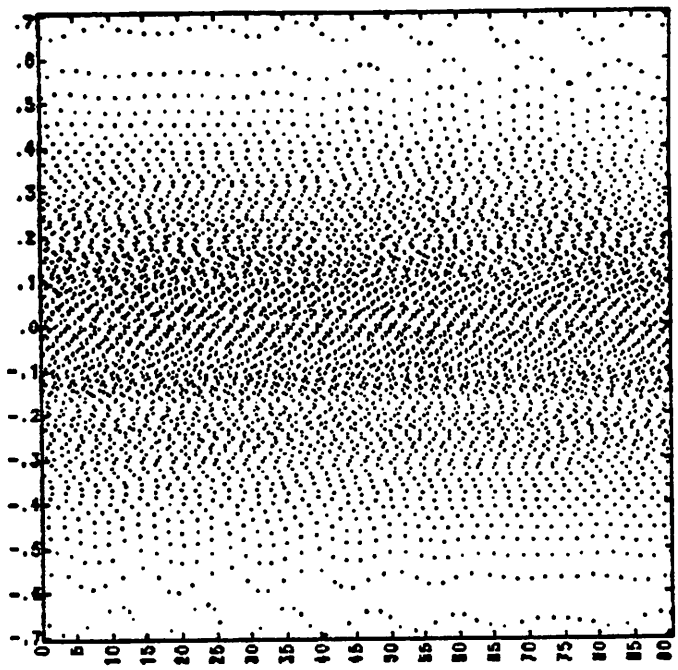

v vs. x

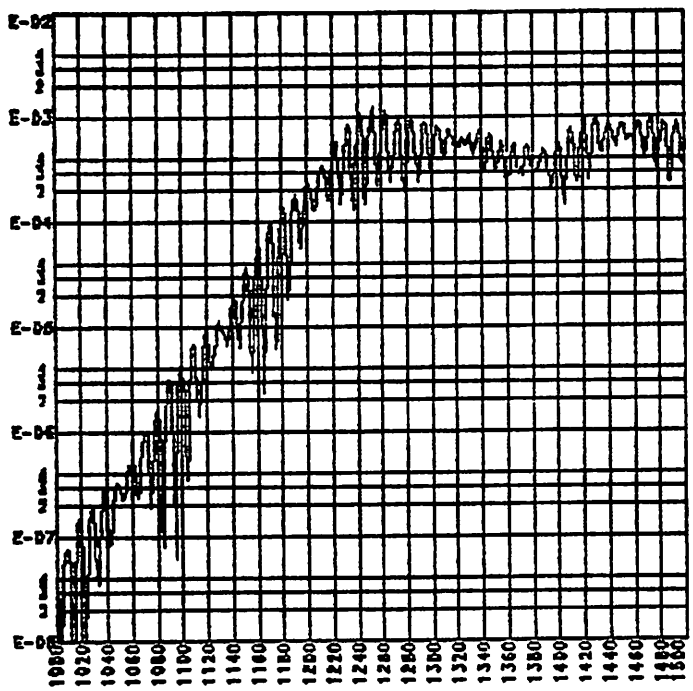

Electric field energy vs. t.

Fig. 5. Growth of the unmagnetized Maxwellian multibeaming instability.

5.2. The Magnetized Maxwellian

When a magnetic field is present, the loading scheme becomes more complicated. Those particles which all have the same total velocity can no longer be called "beams", but could better be termed "rings". The term beam can now be restricted to a set of one or more particles which have the same total velocity and the same gyrophase angle. In the magnetic case, a beam is merely the intersection of a ring and a spoke, so rings and spokes can be made up of many beams each. When there are no particles at a ring-spoke intersection, as was sometimes the case in the loading schemes considered in this project, the rings and spokes are poorly defined.

This was the case in the loading scheme used previously in the warm ring simulation and in Sec. 4.2.3 for the saturation simulations. In both of these cases each ring consisted of a set of one or more particles positioned at a single gyrophase angle. Similarly, each spoke consisted of a set of one or more particles positioned at a single perpendicular velocity.

5.2.1. The Ring-Spoke Loading Schemes

In the ring-spoke loading scheme, each ring consisted of a number of beams (*nplg*), all with the same perpendicular velocity and evenly distributed in gyrophase. Each spoke consisted of a number of beams (*nvlg*), all with the same gyrophase angle but with different perpendicular velocities. A typical arrangement of 16 rings and 32 spokes is shown in Figure 6. The position of the particles was assigned using the bit-reversed loader, with all the beams loaded from the same sequence of bit-reversed numbers. A diagram clarifying this loading scheme sequence is presented in Figure 7, where **A**, **B** and **C** indicate the sequence in which the loading takes place. Each beam was completely loaded before the next one was begun (**A**, in Figure 7), starting from the highest velocity beam in a spoke and working inward (as shown by **B** in Figure 7). In this way each spoke was loaded in turn, so that all the beams were loaded in each spoke before the next spoke was begun (sequence **C** in Figure 7). The loading sequence was important since in all the cases considered in this project, the number of rings, spokes and particles per beam was a power of two. This was used mainly because of convenience, even though it caused undesirable correlations when a loading sequence such as **BAC** was used, which caused particles in the rings to be bunched. Since the bunching was caused by not completely filling a "beam" before moving on to the next one, the only other acceptable loading sequence would be **ACB**.

The number of particles per cell in the beams was more important than the number of spokes or the number of rings. As the number of rings was decreased the results of the simulations resemble those expected from the theoretical predictions for the Maxwellian distribution less and less, but only gradually without any abrupt loss of stability. A similar result was obtained when the number of spokes was decreased. However, when the number of particles in a beam was decreased to one for every two grid cells ($ng/n = 2$), the highest mode number possible ($k = ng/2$) was excited; fortunately this mode is usually was not a growing mode. When the number of particles was reduced further to one for every four grid cells ($ng/n = 4$), the mode which was half the highest possible ($k = ng/4$) was excited; the distribution lost its original order, though only in (v_p, θ_v) space. The excited modes quickly reached a saturation level in the first few time steps approximately proportional to the $1/N_D$ thermal fluctuation level, beyond which no growth occured. The best way to describe the result would be to say that the distribution was unstable in velocity space, but stable in position space: the order in velocity space becomes randomized, while the distribution remains ordered in position space. The velocity of the beams changed drastically, while the beams as a whole remained intact (all the particles in a beam continued to have identical velocity components) and the distribution of the particles of the beams in position space remained uniform.

The loading schemes used to simulate a Maxwellian in this section will therefore presume that there are sufficient particles per beam to prevent the excitation of the previously discussed modes, unless otherwise specified. The main goal will be to confirm the dependency of the

stability on the number of rings and spokes, as derived by *Kim* in QPR II 80[5] and by *Otani*, *Cohen* and *Gerver* in QPR IV 80[6]. In these articles the conditions derived for the stability of the rings and spokes loading were, approximately (for continuous rings),

$$N_{rings} > \frac{1}{3}\left(\frac{\omega_p}{\omega_c}\right)^2$$

and (for rings composed of discrete spokes)

$$N_{spokes} > (8\, k_{\max} v_{th}/\omega_c)$$

where $k_{\max} = \pi\, ng/L$ denotes the maximum value of k. These two conditions would then indicate that

$$N > N_{rings} N_{spokes} N_{beam} = \frac{8}{3}\left(\frac{\omega_p}{\omega_c}\right)^2 \left(\frac{k_{\max} v_{th}}{\omega_c}\right) N_{beam}$$

must be satisfied for numerical stability. Here N_{beam} is used to denote the number of particles per beam, which is equal to the number of grid cells in the $nlg = ng$ case. So if a simulation is desired out to $k_{\max} v_{th}/\omega_c = 30$, then it would be necessary to have $N = 80\,\omega_p^2/\omega_c^2 N_{beam}$ particles, to avoid numerical instabilities.

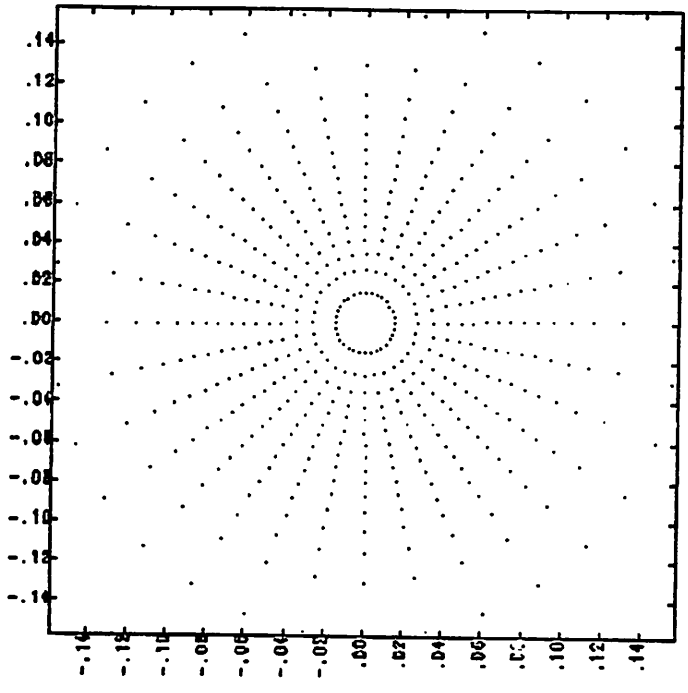

v_y vs. v_x

Fig. 6. A Magnetized Maxwellian distribution represented by 16 rings and 32 spokes.

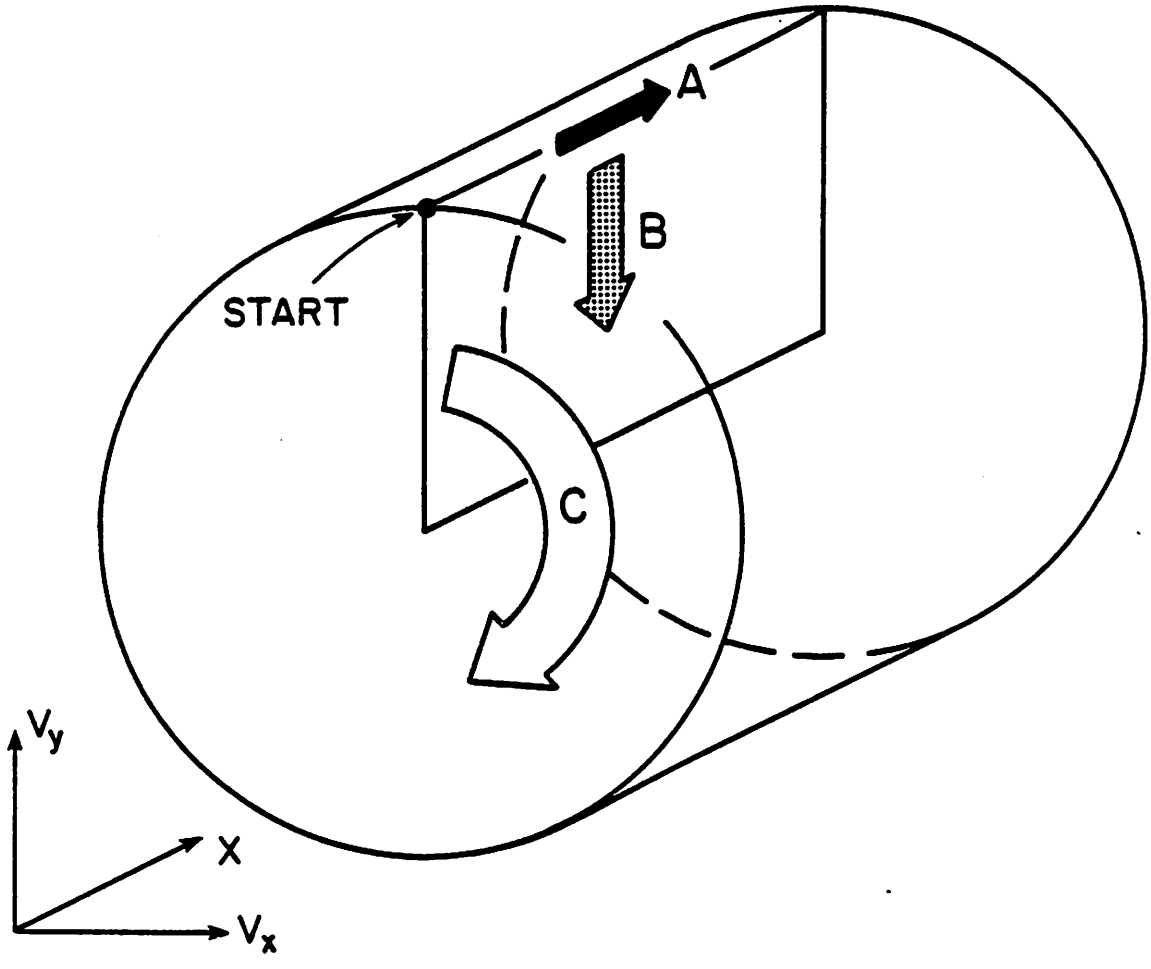

Fig. 7. Loading sequence for the Ring-Spoke loading scheme.

5.2.2. The Ring-Spoke Maxwellian Instability Threshold Results

To test these conditions, it was necessary to find the critical ω_p^2/ω_c^2 as the number of rings or spokes was varied. A grid of 1024 cells was chosen initially to provide enough room for all of the growing modes which might be present. The grid was later reduced to 128 cells when it was found that this was sufficient as none of the higher modes were growing and all of the lower growing modes were allowed.

Since the stability criterion for the minimum number of rings in a Maxwellian distribution assumes that the rings are continuous, the verification of the relation which predicts the minimum number of spokes must be tested first. It was decided to choose a number of rings, say 8 or 32, and then vary the number of spokes from around 8 to 64. In this way any variation of the results due to the number of rings could also be observed in order to see if it was worthwhile to increase the number of rings.

The general trend as more spokes were added was for the critical stability level of ω_p^2/ω_c^2 to rise, with the rise becoming faster after the number of spokes had become greater than 16. When an insufficient number of spokes were used to simulate a continuous ring, the critical stability level of ω_p^2/ω_c^2 was lower than predicted. This was true regardless of how many rings were used, at least up to the maximum that was possible (64). However, when the number of spokes was increased beyond a certain point, the stability was greater than predicted for continuous rings (an infinite number of spokes). This critical number of spokes depended on the number of rings; for 8 rings it was about 16 spokes and for 32 rings it was closer to about 32 spokes. It was thus possible to produce loadings which were more stable than predicted by the theory, though only if enough spokes were used.

The number of grid cells could not be reduced below 128 without reducing the accuracy of the simulation, due to the necessity of having enough allowed modes to permit all the possible growing modes to appear. Because this meant at least 128 particles were needed in each beam and at least 32 rings were needed to adequately represent the Maxwellian, the number of spokes was limited to 64 or less due to the limit of about a quarter-million particles per simulation run. The number of spokes could have been increased still further only by correspondingly reducing the number of rings or the number of allowed modes. Because of the cost of the simulation runs with more than 260,000 particles, very few were made compared to those with fewer particles. Thus, the relationship between the stability of the distribution and the numbers of rings and spokes could not be as fully explored for the cases with larger numbers of rings and spokes as for the cases with fewer rings and spokes.

In order to explore the relationship between the number of rings, the number of spokes and the stability of the distribution a fixed number of rings was chosen for which the stability threshold was found at different numbers of spokes. To find the dependency of the results on the number of rings, two different series of runs were made, one with 8 rings and the other with 32 rings. The result was that the distribution with 32 rings had a higher value of $(\omega_p^2/\omega_c^2)_{crit}$ at any particular number of spokes, as shown in Figure 8.

To allow the number of rings to be varied through a wide range, a case was chosen in which each ring consisted of only one beam. Instead of having all the beams lined up to form a single spoke as would have been the case if the standard loading routine was used, they were bit-reversed in gyrophase angle. The critical ω_p^2/ω_c^2 for stability was then found for different numbers of rings. The resulting relation between $(\omega_p^2/\omega_c^2)_{crit}$ and N_{rings}, as shown in Figure 9, was of course different from that predicted for continuous rings, but only in the magnitude of the values of $(\omega_p^2/\omega_c^2)_{crit}$.

An indication of where the critical threshold would be for $N_{spokes} = 8$, 16 or 32 was gained by graphing the appropriate points from Figure 8 onto Figure 9. Since two points were not enough to more than roughly indicate the dependency of the stability on the number of rings at the higher numbers of spokes, more points were determined to clarify the relationship. It can be seen that with the number of spokes equal to 32, the stability threshold is greater than that predicted by theory (both the simple relation and the more rigorous theory), though it is

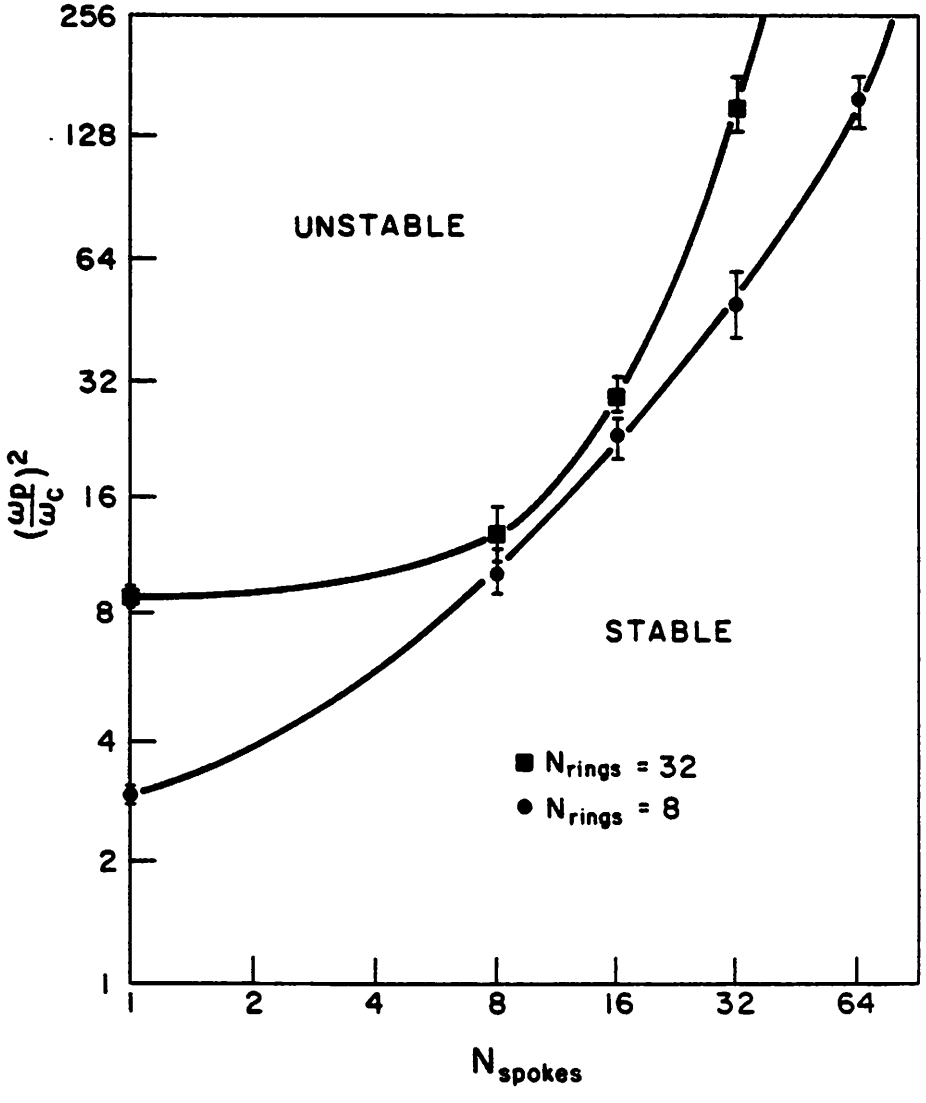

Fig. 8. Magnetized Maxwellian instability threshold for $N_{rings}=8$ and 32, as a function of N_{spokes}, bit-reversed in velocity space phase angle.

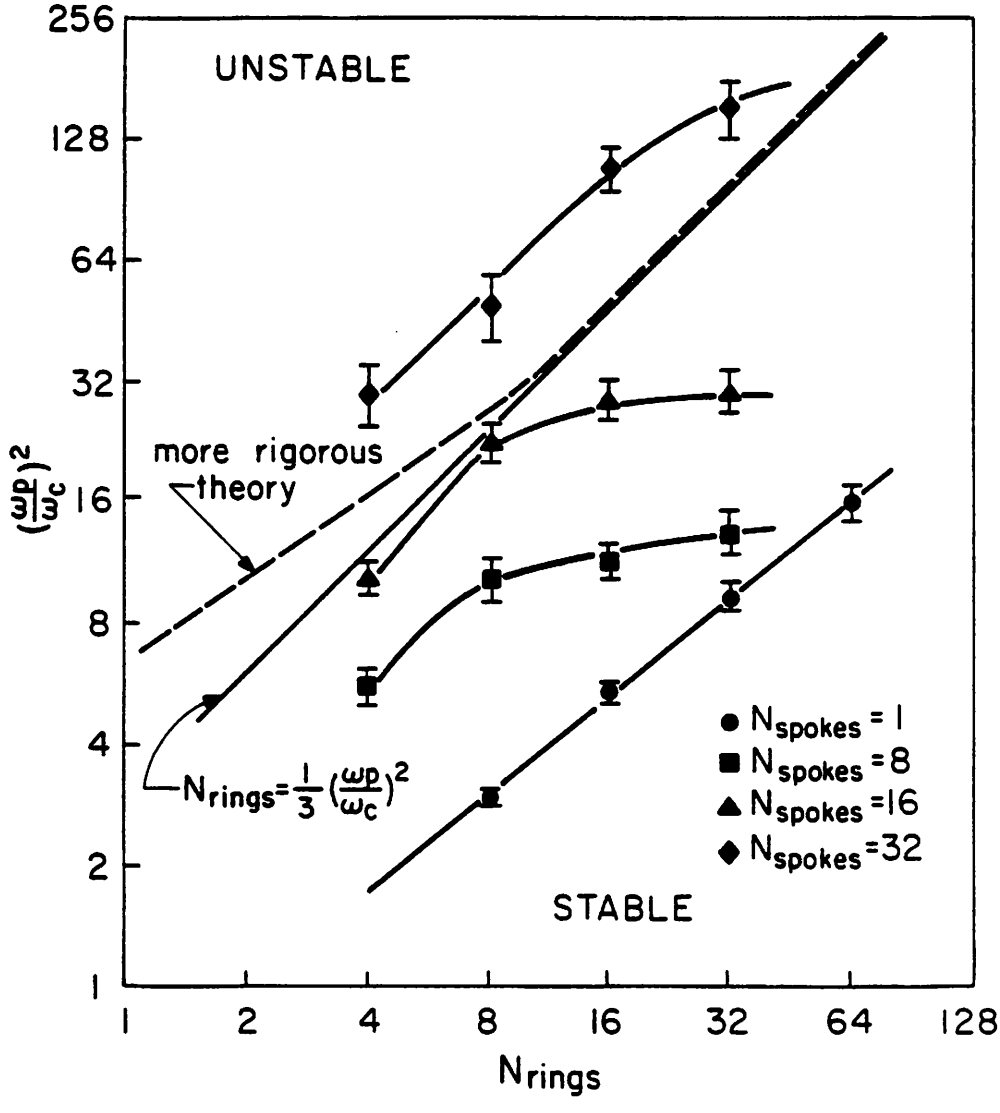

Fig. 9. Magnetized Maxwellian instability threshold for $N_{spokes}=1,8,16$ and 32, as a function of N_{rings}, bit-reversed in velocity space phase angle.

roughly proportional to it. It can also be seen from Figure 9 that for $N_{spokes} = 8$ and 16, the dependency of the stability threshold on the number of rings is weaker for the larger number of rings.

5.3. Saturation Results

In this section the growth of the electric field energy to saturation (presumably at the thermal fluctuation level) was investigated. Since a quiet start of the level that could be achieved with one particle per cell in each beam was not needed, each beam was allowed to consist of only one particle. There was also only one particle per ring and one particle per spoke so that each particle occupied a unique (x, v_p, θ_v) position. This style of loading scheme was sufficient in this case since it was not important how quickly the electric field saturated but at what level. The saturation levels of this loading scheme and of the previous (ring-spoke) loading schemes were approximately the same, depending only on the total number of particles, though not all the simulation runs were run long enough for the field energy to saturate because of the expense. The saturation level was expected to be proportional to some power of $1/N_D$ where $N_D = n\, v_{th}/\omega_p$. This configuration was tested with a strong magnetic field ($\omega_p^2/\omega_c^2 = 10$) and a weak magnetic field ($\omega_p^2/\omega_c^2 = 400$).

5.3.1. The Saturation Loading Schemes

All of the possible combinations of the different loading schemes were used; bit-reversed, trit-reversed and random in position space and gyrophase angle space. The simulation results are summarized in table 1 for $\omega_p^2/\omega_c^2 = 400$. Figures 10 and 11 are v_y vs. v_x plots of the bit-reversed and trit-reversed gyrophase angle loadings, respectively, at $t = 0$, with $v_{th} = .5$. Each particle in these loadings has its own position in velocity phase space. The loading scheme used for particle positions was more important than the gyrophase angle loading scheme, because only the *position* determines the mode excitation levels. This caused the initial mode energy plots to be identical if the position loading was the same, though the distribution of the mode energy changed in later plots due to the influence of the gyrophase angle loading. This meant that if a loading in position space was poor, it was very unlikely that there was a gyrophase angle loading that would improve the results.

In all the Magnetized cases in which a Maxwellian distribution was loaded, the perpendicular velocities ($v_\perp = v_p$) were chosen using the inverse linear interpolation of the velocity integral. In **ES1**, the parameter $NV2$ was set equal to 1, producing a thermal velocity distribution. The particle velocities were chosen such that the v_is satisfied the integral equation

$$\frac{i}{N} = \frac{\int_{-\infty}^{v_i} e^{-v_\perp^2/2v_{th}^2} 2\pi v_\perp dv_\perp}{\int_{-\infty}^{\infty} e^{-v_\perp^2/2v_{th}^2} 2\pi v_\perp dv_\perp}$$

for the respective values of i.

5.3.2. The Weakly Magnetized Case

The first case tried was with a weak magnetic field; $\omega_p^2/\omega_c^2 = 400$. The loading scheme chosen was the best of the ones tried in the preceeding section; bit-reversed in position and trit-reversed in gyrophase angle. This had the advantage of a smooth rise of the electric field energy of about 2 orders of magnitude to a fairly stable saturation level, as shown in Figure 12 for $n = 32768$. For comparison, Figure 13 is a history plot of the electric field energy,

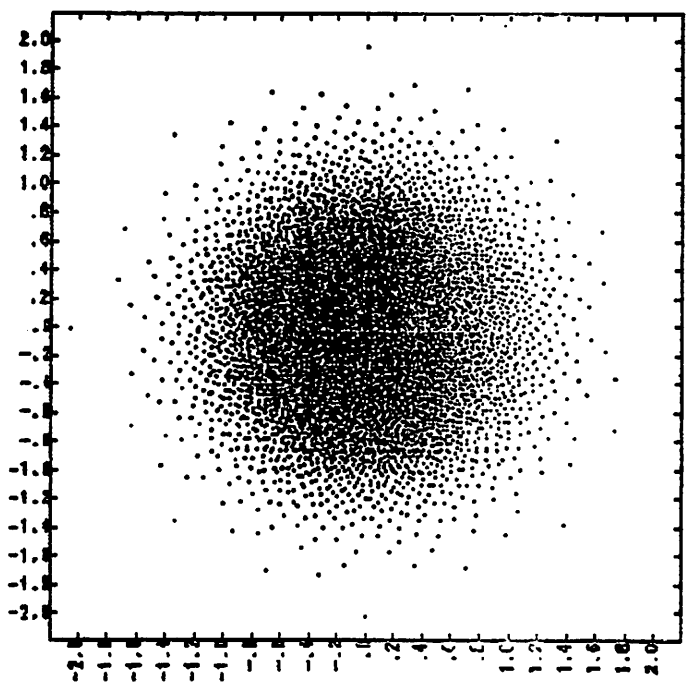

v_y vs. v_x

Fig. 10. Projection of all particles in $v_x - v_y$ space for bit-reversed in velocity space phase angle loading scheme.

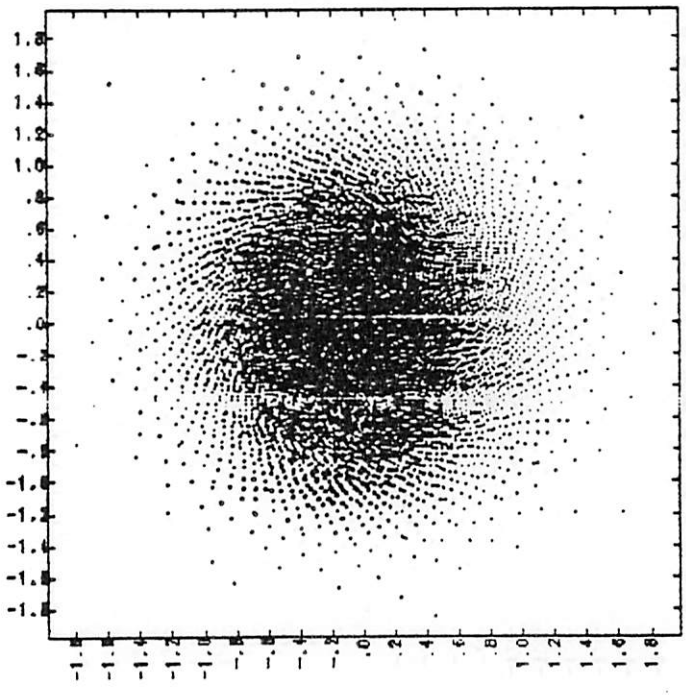

v_y vs. v_x

Fig. 11. Projection of all particles in $v_x - v_y$ space for trit-reversed in velocity space phase angle loading scheme.

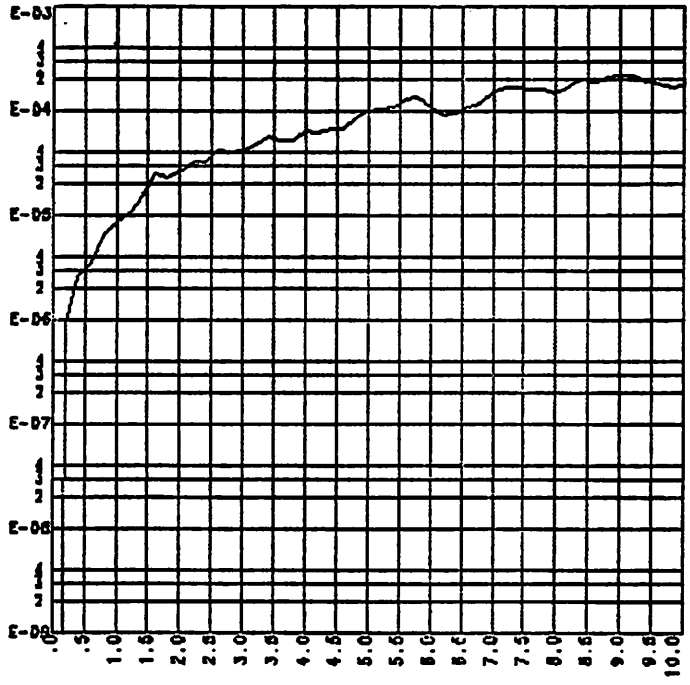

E_{field}/E_{total} vs. t

Fig. 12. Weakly magnetized bit-trit field energy saturation evolution for $\omega_p^2/\omega_c^2 = 400$, $n = 32768$.

$E_{field}/KE_{t=0}$ vs. t

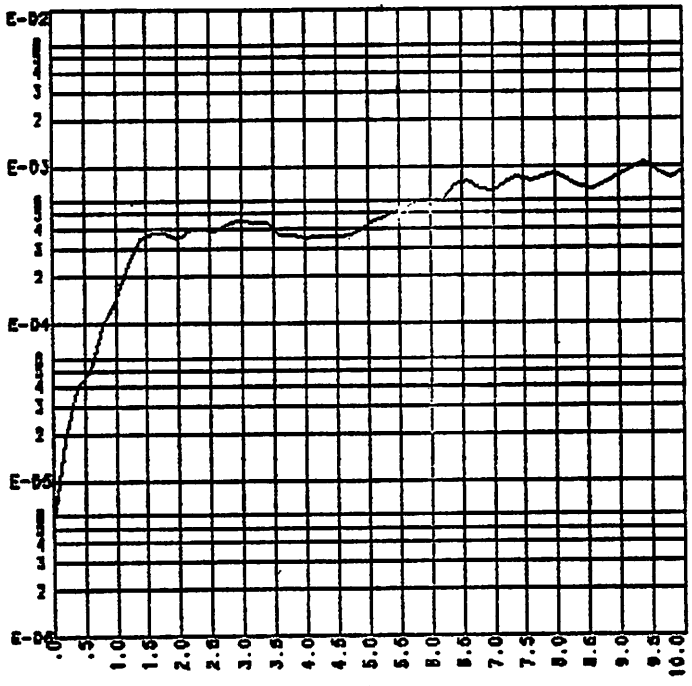

E_{field}/E_{total} vs. t

Fig. 13. Weakly magnetized trit-bit field energy saturation evolution for $\omega_p^2/\omega_c^2 = 400$, $n = 8192$.

$E_{field}/KE_{t=0}$ vs. t

Table 1.

	Velocity Phase Angle		
Position	Bit-Reversed	Trit-Reversed	Random
Bit-Reversed	BAD: A strong mode 1 component due to the correlation. The initial normalized electric field energy is very low $<10^{-27}$, but jumps to 10^{-2} on the first time step.	GOOD: No single strong mode and with a smooth rise as t^2 to the saturation level of approx. 10^{-3}.	POOR: Initial jump to $>10^{-4}$ and then fast rise to saturation at 10^{-3}.
Trit-Reversed	FAIR: Similar to bit-trit, except every ninth mode is excited and the rise from the initial level of approx. 10^{-5} to the saturation level is rather abrupt.	BAD: Similar to the bit-bit loading with the same strong mode 1 component but with a more abrupt rise to the saturation level.	POOR: Virtually identical to the bit-random loader.
Random	POOR: Initial field energy level virtually equal to the saturation level. The field energy oscillates around the saturation level with a variation of about a factor of 4 and a slight decay of the magnitude of the oscillations.	POOR: Virtually identical to the random-bit loader.	POOR: A strong mode 1 component and an oscillating field energy saturation level.

obtained using the trit-reversed in position, bit-reversed in gyrophase angle loading scheme, with $n = 8192$. The electric field energy, along with all the other energies measured by the code in the history plots, was normalized with respect to the initial total energy $(ESE_o + KE_o)$, which was virtually equal to the kinetic energy since the initial electric field energy was never more than about one percent of the initial kinetic energy.

To find the relationship between the electric field energy saturation level and N_D, a series of runs were made with all inputs identical except for the number of particles, which was doubled on each succeeding run. The runs were made with $n = 8192$ to 262144 particles (2^{13} to 2^{18}). The initial rise of the electric field energy was found to be roughly proportional to t^2. The saturation level was found to be proportional to $1/N_D$ as shown in Figure 14, though it was not equal to $1/N_D$ as was derived on pages 74-76 of *Krall and Trivelpiece*[7].

5.3.3. The Strongly Magnetized Case

In the next case ω_p^2/ω_c^2 was set equal to 10, (i.e. the strong magnetic field case). The same set of runs was made as in the weakly magnetized case to observe if there was any difference in the relation between the saturation level of the electric field energy and n. The growth of the electric field energy was roughly proportional to t^2 and the saturation level was now observed to be roughly proportional to $(1/N_D)^2$, though at a higher overall level as is shown in Figure 15.

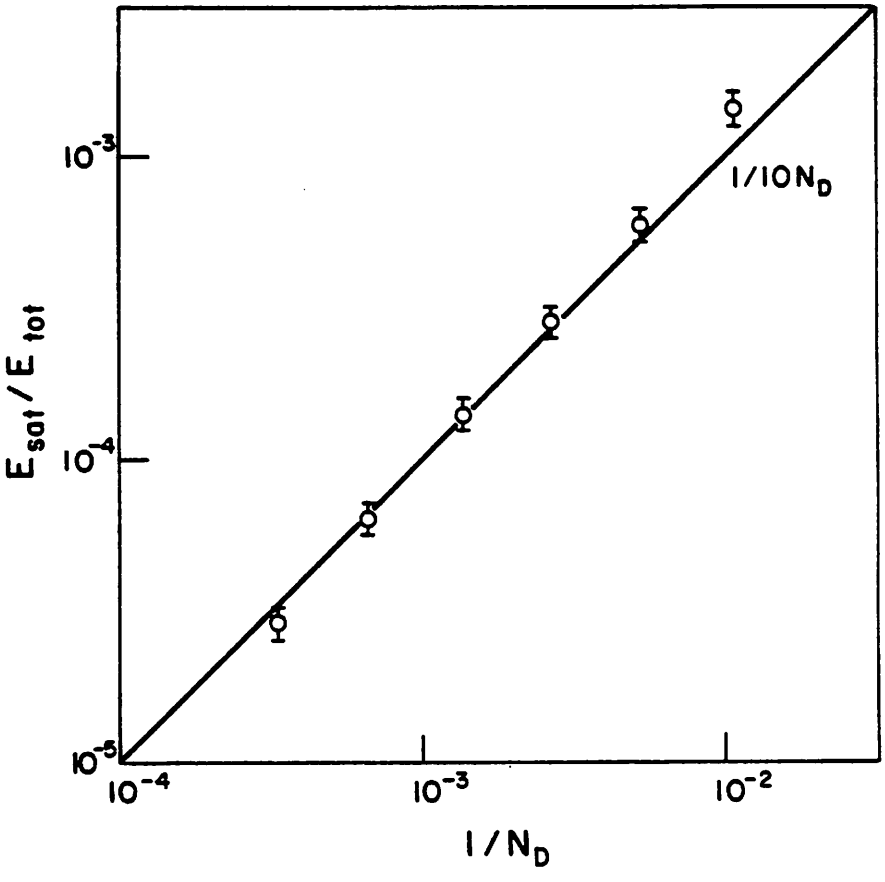

Fig. 14. Weakly magnetized ($\omega_p^2/\omega_c^2 = 400$) saturation level.

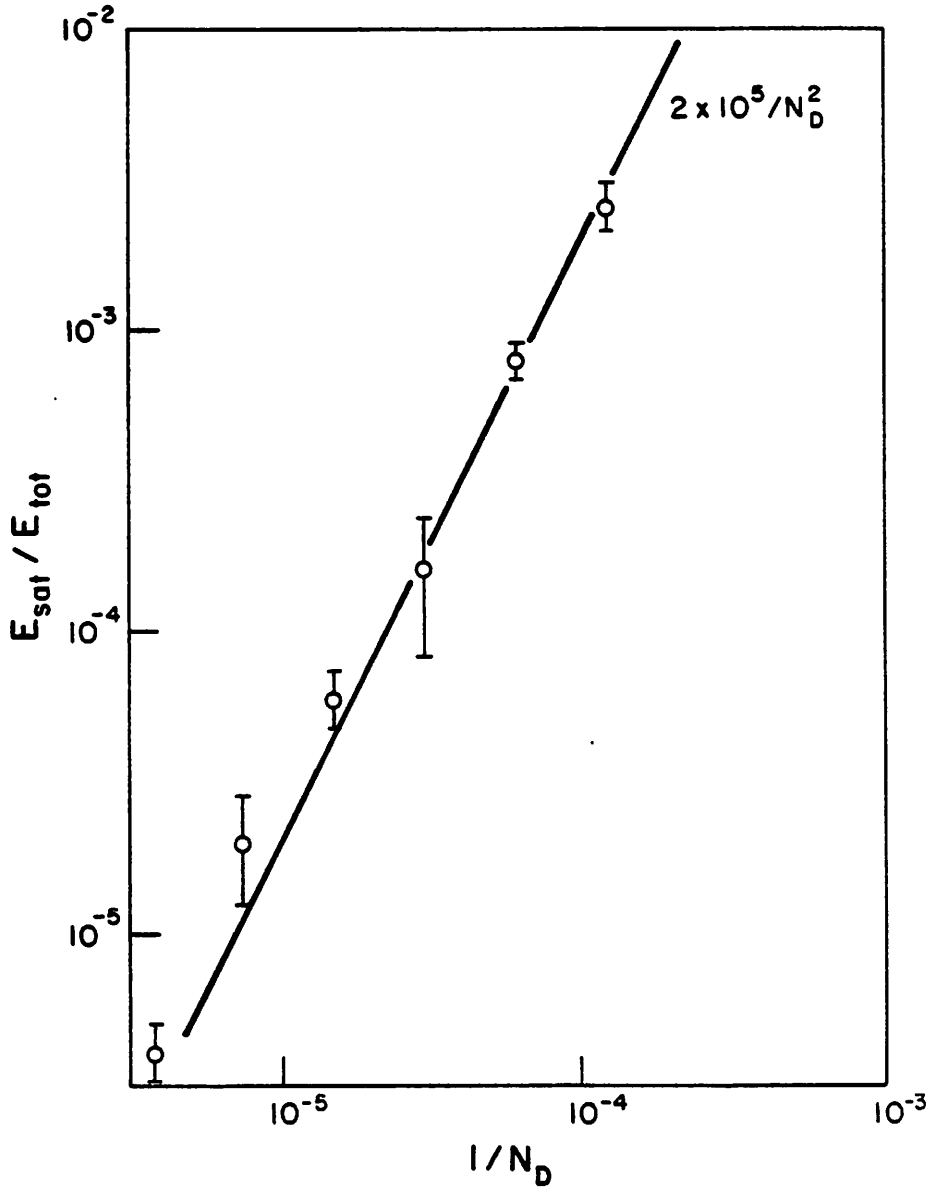

Fig. 15. Strongly magnetized ($\omega_p^2/\omega_c^2 = 10$) saturation level.

6. Summary

As the primary subject of this paper is that of different loading schemes for a Maxwellian distribution, it cannot be overemphasized that there are many different distinct loading schemes, and many different ways of loading each distinct scheme. As occurred in this project, two different routines for loading virtually the same arrangement of particles produced results which were nearly identical but not quite. Because of the three coordinates over which the particles must be distributed, the various permutations of the different loading schemes can become extremely complex, with unexpected correlations between the loading routines for each coordinate.

The simplest kind of loading scheme gives each particle a unique position in each of the three coordinates; there is only one particle per ring, one particle per beam, and one particle per spoke. Using this condition, many different kinds of routines can be used to load the actual positions, such as: ordered, bit-reversed, trit-reversed, etc. Once the particles had been "loaded," various methods could be used to mix them to remove correlations or repeated sequences, such as "twisting" the particles in velocity space about the zero velocity axis, as is shown in Figure 14. This basic loading scheme was used with various combinations of loading routines, and found to have a basic problem in which the electric field energy jumped from an extremely low ($\sim 10^{-27}$ of K.E.) initial value to a value near 10^{-6} or 10^{-5} of K.E. on the first time step. The electric field energy then rose relatively slowly to saturate finally at a value which was roughly proportional to $1/N_D$ or a power of $1/N_D$. The problem with this loading scheme as a whole was that the initial rise was fairly short, even for the best of the combinations of routines, approximately 25 time steps or less (see Figure 10 (MS report version)).

The next logical step was to increase the number of particles per ring, spoke, or beam. This complicated the loading schemes enormously and, consequently, the number of tests was proportionately smaller. The number of particles also increased quickly, especially if some theoretical predictions were to be tested rigorously. It was found, however, that it was possible to load the particles in such a way that the electric field energy grew from a very low initial level (approximately 10^{-27} K.E.) at a rate determined by the value of $(\omega_p/\omega_c)^2$. Below a minimum value of $(\omega_p/\omega_c)^2$, the simulation was stable, while above that level, the electric field grew many orders of magnitude to a final saturation level. It can only be presumed that this final saturation level was proportional to $1/N_D$ as before, as it was prohibitively expensive to follow more than a very few runs all the way out to saturation because of the large number of particles. The key observation of this phase of the project was that it was almost always necessary to have one particle per grid cell in each beam to avoid the presence of unwanted modes.

While the number of particles per beam leaves the velocity distribution function unchanged, the number of particles per spoke and the number of particles per ring change the form of the velocity distribution function. For example, the number of particles per spoke is equal to the number of rings and vice versa. The first simulations were run with only one ring; this resulted in the velocity distribution functions shown in Figure 15, where two different ways of looking at the distribution are shown: $f(v_x)$ and $f(v_p)$. These are the integrations of the velocity function over v_p and v_x. The same "views" of a Maxwellian distribution ($f(v_x)$ and $f(v_p)$) are shown in Figure 16. This distribution function is what would result if the number of spokes were infinite (continuous rings) and the number of rings are infinite. Neither of these conditions could of course be satisfied, so the actual distributions were not quite as smooth as those shown in Figure 16.

REFERENCES

[1] H. S. Au-Yeung and Y-J. Chen, *Plasma Theory and Simulation Quarterly Progress Report*, IV, 14, (1980), **ERL**, UC Berkeley, CA.

[2] **Unstable electrostatic plasma waves propagating perpendicular to a magnetic field**, R. A. Dory, G. E. Guest and E. G. Harris, *Phys. Rev. Letters*, **14**, 131, (1965).

[3] **Cyclotron harmonic wave propagation and instabilities**, J. A. Tataronis and F. W. Crawford, *J. Plasma Physics*, **4**, 231, (1970).

[4] **Multibeam instability in a Maxwellian simulation plasma**, S. J. Gitomer and J. C. Adam, *Phys. Fluids*, **19**, 719, (1976).

[5] J. S. Kim, *Plasma Theory and Simulation Quarterly Progress Report*, **II**, 4, (1980), **ERL**, UC Berkeley, CA.

[6] N. Otani, B. I. Cohen and M. J. Gerver, *Plasma Theory and Simulation Quarterly Progress Report*, **IV**, 3, (1980), **ERL**, UC Berkeley, CA.

[7] N. A. Krall and A. W. Trivelpiece, **Principles of Plasma Physics**, *McGraw-Hill*, New York, 1973.